Ablation of Proliferating Osteoblast Lineage Cells After Fracture Leads to Atrophic Nonunion in a Mouse Model

Katherine R. Hixon[1] PhD, David A.W. Sykes[2] BS, Susumu Yoneda[1] MD, Austin Hensley[1,3] MS, Evan G. Buettmann[1,3] PhD, Dimitrios Skouteris[1] MD, Jennifer A. McKenzie[1] PhD, Anna N. Miller[1] MD, and Matthew J. Silva[1,3] PhD

[1]Department of Orthopaedic Surgery; [2]Department of Biology; [2]Department of Biomedical Engineering; – Washington University in St. Louis

Running Title: 5 words max

Fracture Healing Requires Proliferating Osteoblasts

Corresponding Author:

Katherine Hixon

BJCIH 11th Floor, RM 11302

Campus Box 8233

Orthopaedic Surgery

(314) 747-6070

khixon@wustl.edu

ABSTRACT

Nonunion is defined as the permanent failure of a fractured bone to heal, often necessitating surgical intervention. Atrophic nonunions are a subtype that are particularly difficult to treat. Animal models of atrophic nonunion are available; however, these require surgical or radiation induced trauma to disrupt periosteal healing. While these approaches can result in nonunion, such invasive methods are not representative of many clinical nonunions where osseous regeneration has been arrested by a “failure of biology”. We hypothesized that arresting osteoblast cell proliferation after fracture would lead to atrophic nonunion in mice. Using mice that express a thymidine kinase (tk) ‘suicide gene’ driven by the 3.6Col1a1 promoter (Col1-tk), proliferating osteoblast lineage cells can be ablated upon exposure to the nucleoside analog ganciclovir (GCV). Wild-type (WT; control) and Col1-tk littermates were subjected to a full femur fracture and intramedullary fixation at 12 weeks old. Post injury, mice were dosed with GCV twice daily for 2 or 4 weeks. Histologically, we confirmed abundant tk+ expression in fracture callus, and diminished periosteal cell proliferation in Col1-tk mice at 3 weeks post fracture. Moreover, Col1-tk mice had less osteoclast activity, mineralized callus, and vasculature at the fracture site compared to WT mice. Additional mice were monitored for 12 weeks with *in vivo* radiographs and microCT scans, which revealed delayed bone bridging and reduced callus size in Col1-tk mice. Following sacrifice, *ex vivo* microCT and histology demonstrated failed union with residual bone fragments and fibrous tissue in Col1-tk mice. Biomechanical testing demonstrated an inability to recover torsional strength in Col1-tk mice compared to WT. Our data indicates that suppression of proliferating osteoblast-lineage cells for either 2 or 4 weeks after fracture blunts the formation and remodeling of a mineralized callus leading to a functional nonunion. We propose this as a new murine model of atrophic nonunion.

Five Key Words: Injury/Fracture Healing, Genetic Animal Models, Biomechanics

Introduction

Nonunion is defined as the permanent failure of a fractured bone to heal, where surgical intervention is often required to achieve healing [1]. The reported clinical rate of nonunion is 5%; thus, an estimated 500,000 fractures result in nonunion in the United States each year [2-4]. Due to the necessary advanced care, treatment can cost upwards of $90,000 per individual [5]. Nonunions are caused by a variety of factors such as infection, avascularity, or lack of stability, and are broadly categorized as hypertrophic or atrophic, each of which require different treatment options [1, 6]. Of these, atrophic nonunion is the least understood and the most difficult to treat [6, 7]. The majority of animal models available for atrophic nonunion involve local periosteal stripping, bone marrow removal, devascularization, or the creation of a critical-sized defect [6, 8]. Despite their prevalence as models of nonunion, such invasive methods are not representative of many clinical nonunions which are instead due to the disturbance of biological pathways [1, 9]. Thus, there is an unmet need for a clinically relevant “failure of biology” atrophic nonunion animal model in which therapeutic interventions could be tested.

Fracture healing in mice and humans is very similar, wherein both endochondral and intramembranous ossification contribute to new bone formation. In healthy mice, complete bridging of the fracture site with bony callus occurs 3-4 weeks after fracture [10, 11]. In humans, fractured long bones typically heal within 2-3 months and nonunions are clinically diagnosed after 6-9 months of nonhealing, i.e., 3-times the normal healing time [10, 12]. Thus, it has been proposed that a conservative assessment of nonunion in mice should be based on evaluation at 12 weeks post fracture [10, 13].

Proliferation of periosteal cells occurs during fracture healing, providing a source of callus osteoblasts and chondrocytes [6, 14-16]. Previous work in rodents has shown that cell proliferation in periosteal callus is elevated as early as 2 days and remains elevated through 12-14 days after fracture, as shown by expression of proliferating cell nuclear antigen (PCNA) [17-19]. However, while the progression of proliferation during fracture healing has been identified, the exact molecular identity of these contributing cells remains unclear. These observations suggest that the first 2 weeks are a critical period for proliferation during rodent fracture healing. They further suggest that impaired cell proliferation during this period will lead to blunted callus formation, which may in turn result in atrophic nonunion. To our knowledge, whether proliferation of periosteal progenitors in the early post-fracture period is required for successful healing has not been proven.

Recent reports on the molecular identity of periosteal progenitors that contribute to fracture callus have used lineage tracing to identify a number of non-unique genes that mark this population [20]. Earlier work demonstrated high GFP reporter expression in periosteal cells of 3.6Col1a1-GFP mice and showed that 3.6Col1a1 marks cells of the osteoblast lineage [21]. We recently reported that proliferation of the 3.6Col1a1 cell population contributes to periosteal bone formation after non-injurious mechanical loading [22], leading us to hypothesize that this population may also be critical to fracture healing, which is largely a periosteal-driven process [23]. Jilka et al. [24] developed 3.6Col1a1-tk (Col1-tk) mice in which proliferating osteoblast lineage cells can be ablated through exposure to the nucleoside analog ganciclovir (GCV). Specifically, in the presence of GCV, replicating cells expressing a thymidine kinase (tk) ‘suicide gene’ convert GCV to a toxic nucleotide which is incorporated into the DNA of 3.6Col1a1 expressing cells resulting in targeted cell death [24]. This

model provides a unique tool to test the requirement of proliferation of a defined population of periosteal cells to fracture healing.

The central hypothesis of this study is that proliferation of periosteal osteoblast-lineage cells is required for fracture healing. We created midshaft femur fractures in young-adult Col1-tk mice, and treated them with GCV for 2 or 4 weeks to ablate proliferating osteoblast-lineage cells, followed by withdrawal. Wildtype (WT) littermate control mice were treated identically. Healing was assessed by *in vivo* serial radiography and microCT, followed by terminal assessment at 3- and 12-weeks post fracture using histology, microCT and mechanical testing. Our findings show that suppression of proliferating osteoblast-lineage cells for either 2 or 4 weeks after fracture blunts the formation and remodeling of a mineralized callus leading to a functional nonunion. We propose this as a novel “failure of biology” murine model of atrophic nonunion.

Materials and Methods

Mouse Lines

A total of 132 male and female mice at 12 weeks of age were used. All experimental procedures were approved by the Institutional Animal Care and Use Committee (IACUC) at Washington University in St. Louis in accordance with the Animal Welfare Act and PHS Policy on Humane Care and Use of Laboratory Animals. Transgenic 3.6Col1A1-tk (Col1-tk) mice (provided by Drs. Robert Jilka and Charles O’Brien) were used to target replicating osteoblast progenitors [24]. Specifically, these mice were developed to express the herpes simplex virus thymidine kinase (HSV-tk, or ‘tk’ for short) gene, driven by the 3.6 kb rat Col1A1 promoter which is active in osteoblast lineage cells. In the presence of the nucleoside analog ganciclovir (GCV), replicating osteoblast progenitors expressing thymidine kinase (tk) convert GCV to a toxic version of the nucleotide which is then incorporated into the DNA of 3.6Col1a1 expressing cells. Following integration, the DNA strands break, resulting in cell apoptosis [24]. To generate Col1-tk mice, male C57BL6/J (The Jackson Laboratory, #000664) mice were bred to female mice heterozygous for the tk transgene (tk-positive). This resulted in both heterozygous tk-positive (Col1-tk) and tk-negative (wildtype, WT) mice. Note that only one allelic copy of the tk transgene is necessary, and male Col1-tk mice are sterile. Genotyping was completed by Transnetyx using toe biopsies from the mice for real-time PCR (probe: puro). Subsequent breeding was completed using littermates (Col1-tk females and tk-negative (WT) males). All mice were group-housed with up to five mice per cage under standard 12-hour light/dark cycle and given full access to food and water. Breeders were given high-fat chow and after weaning all mice were given normal chow. In a pilot study, two control groups were examined (WT dosed with GCV; and Col1-tk dosed with vehicle (H_2O)); histology and microCT demonstrated that both groups had normal appearing callus, with comparable bone volume and volumetric bone mineral density (most data not shown). We chose WT dosed with GCV as the control group for all subsequent studies. All mice were dosed with ganciclovir (GCV, 8 mg/kg i.p., McKesson, San Francisco, CA) twice daily (**Figure 1A**) starting at

the day of fracture (12 weeks of age). Mice were euthanized by CO_2 asphyxiation at designated endpoints from 1 to 12 weeks after fracture.

Study to Confirm Thymidine Kinase (tk) Expression in Full Fracture Callus

In a subset of mice (n=15), WT mice were dosed with GCV and Col1-tk mice were dosed with either GCV or vehicle (H_2O) for 2 weeks after fracture. Immunohistochemistry on decalcified, paraffin-embedded sections was used to visualize expression of tk in fracture callus as detailed below.

Proliferation Assessment Study

To assess proliferation following GCV drug withdrawal, 5-Ethynyl-2'-deoxyuridine (EdU, 0.2 mg/mL in 5% sucrose) was added daily to the drinking water of two subsets of mice. First, for 2 weeks after fracture mice were treated with GCV but did not receive EdU. During the next (third) week, mice received EdU but not GCV. After this third week, the mice were sacrificed to analyze the cumulative proliferative response (EdU staining) during the week, i.e., the first week after removal of the anti-proliferative conditions (**Figure 1B**). In a second subset, Col1-tk mice were fractured and immediately given EdU with or without the addition of GCV for one week to assess proliferation immediately following fracture (**Figure 1B**). These mice were then sacrificed at this one week timepoint to visualize EdU histologically.

Fracture Healing Study

For the main aim of the study, mice were dosed with GCV following fracture to target both the proliferative phase (2 week dosing) as well as the interval during which normal fracture healing occurs (4 week dosing). Following dosing for 2 or 4 weeks, GCV was then withdrawn and weekly monitoring of fracture healing continued through sacrifice (12 weeks) to evaluate healing (**Figure 1C**). Following euthanasia, animals were randomly assigned to either histological or biomechanical evaluation.

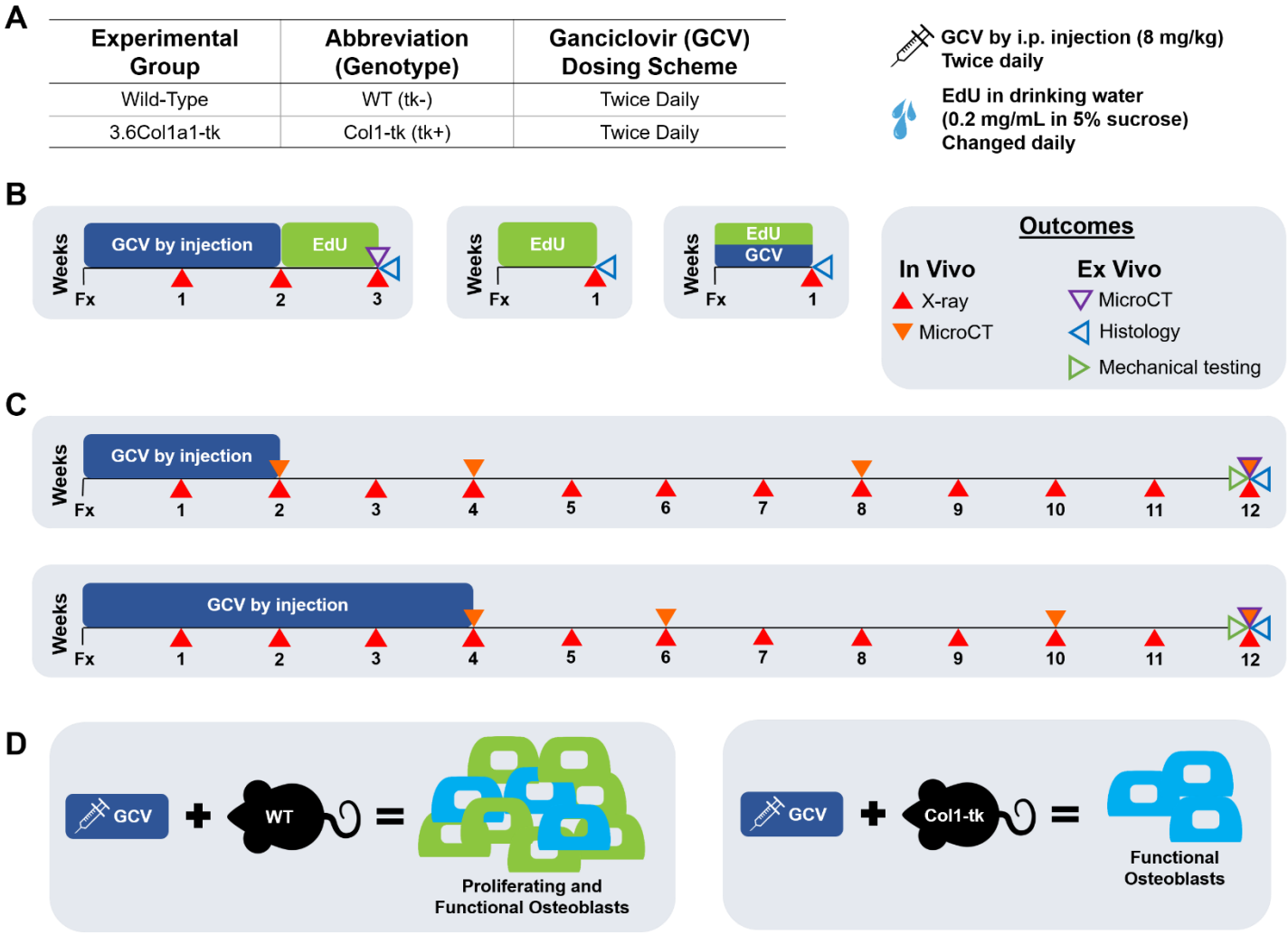

Figure 1. Experimental overview. Unilateral femur fractures were created in mice at 12 weeks age. (A) Both Col1-tk (tk-positive) and WT (tk-negative) mice were dosed with GCV, twice daily. (B) To assess proliferation, mice were dosed for two weeks and then given EdU in their drinking water for an additional week. Outcomes included weekly X-rays as well as microCT and histology post mortem. Another set of Co1-tk mice received 1 week of EdU, starting immediately after fracture, with or without GCV injections. (C) To assess the potential for recovery from suppressed osteoblast proliferation, mice were dosed with GCV for both 2 and 4 weeks before withdrawal, and then assessed by X-rays and *in vivo* microCT until sacrifice at 12 weeks. *Ex vivo* evaluation included microCT, histology, and mechanical testing. (D) In this experimental model, WT mice dosed with GCV have an increase in proliferating osteoblasts in addition to the resident functional osteoblasts. In contrast, Col1-tk mice only have resident functional osteoblasts present due to the ablation of proliferating osteoblasts with GCV administration.

Full Fracture Model

A previously established full fracture protocol was used to induce fracture in the right femur of 12-week-old mice [25]. Briefly, a transverse force was applied across the right femoral mid-diaphysis using a custom 3-pt bending setup (DynaMight 8841; Instron, Grove City, PA, USA) creating a unilateral fracture in the midshaft.

Following injury, the femur was stabilized using a 24-gauge metal pin (MicroGroup, Medway, MA, USA) and the wound closed using 3-0 nylon sutures (Ethicon). Fixation was confirmed by radiograph (Faxitron Ultrafocus 100; Faxitron Bioptics, LLC, Tucson, AZ, USA) immediately following surgery. This model mimics classical fracture injury and healing [26, 27], with both intramembranous bone formation and endochondral healing around the periphery and within the fracture gap, respectively [11, 28].

Radiographic Evaluation

Lateral radiographs were taken weekly following full fracture until euthanasia (3X magnification; Faxitron UltraFocus100; n=12-18/group). All radiographs were blindly scored for the degree of healing using a modified Goldberg score (i.e. 0 = no bridging, 1 = one side bridged, 2 = complete bridging) [29]. Mice were excluded from the study if the pin was missing, unstable within the femur, or if there was loss of fixation during healing (total 18 mice).

Micro-Computed Tomography

In vivo scans were performed at 2, 4, 8, and 12 weeks or 4, 6, 10, and 12 weeks for 2 and 4 weeks of GCV dosing, respectively (n=7-9/group). For each scan, the animal was anesthetized (1-3% isoflurane gas) and both femurs were scanned simultaneously using microCT (VivaCT 40, Scanco Medical AG, Switzerland; 15 µm voxel size, 70 kV, 114 µA, and 300 ms integration time). Due to the artifact from the metal pin, threshold- or density-based measurements using Scanco software could not be performed. The proximal and distal ends of the callus were visualized, and a measurement of 3D distance between the center of the two sections was calculated (mm). Contour lines were drawn around the outer edge of the callus and the callus volume was output as total tissue volume (TV, mm^3). For *ex vivo* scans, femurs were dissected from the surrounding tissue and fracture fixation pins were removed (n=15-18/group). Femurs were scanned using microCT (VivaCT 40, Scanco Medical AG, Switzerland; 10.5 µm voxel size, 55 kV, 145 µA, 300 ms integration time). Analysis regions of interest (ROIs) differed for *ex vivo* 3 and 12 week femurs due to changes in callus length over time. For femurs dissected at 3 weeks (n=12/group), a 600 slice (6.3 mm length) ROI was centered at the midpoint of the fracture line and a threshold of 160 was used. The ROI length was selected to include the entire callus region of all samples. Each callus was contoured around its periphery, and the ROI included the original cortical bone plus the callus. Outcomes were total bone volume (BV, mm^3), tissue volume (TV, mm^3), volumetric bone mineral density (vBMD, mg HA/cm^3), and tissue mineral density (TMD, mg HA/cm^3). At 12 weeks post fracture (n=14-17/group), a region of interest (ROI) of 200 total slices (2.1 mm) was identified, centered at the point of fracture, and the threshold was set to 350. This smaller ROI length reflected the shorter extent of mineralized callus at this timepoint. Due to remodeling of the callus, fracture lines were not visible at 12 weeks, thus the point of fracture was inferred from radiographic images at 2 weeks post fracture (femoral head to fracture midpoint distance). Contours around the periosteal bone surface were drawn and BV, TV,

vBMD, and TMD were determined. Following *ex vivo* scanning, the femurs were either decalcified and processed for histology, or prepared for mechanical testing.

Histological Analysis

To confirm the specific targeting of tk+ cells with GCV, immunohistochemistry (IHC) was used to detect the HSV tk protein at 2 weeks post fracture [24]. Briefly, the paraffin slides were deparaffinized in xylene and rehydrated in graded ethanols. Incubation with 3% H_20_2 (5 min) blocked endogenous peroxidases. Endogenous epitopes were blocked with 10% goat serum (abcam – ab7481) in PBS at room temp (1 hour). The sections were then incubated with rabbit polyclonal anti-HSV tk (1:100; gift from William Summers, Yale) at room temp (3 hours). The secondary antibody incubation and chromogenic HRP development were completed according to manufacturer's instructions (Dako Envision HRP System; K4010). Sections were counterstained with Modified Mayer's hematoxylin (Electron Microscopy Services 26041 – 05) and imaged at 20x on a Nanozoomer slide scanner (Hamamatsu Photonics).

Femurs from mice given EdU designated for frozen processing following fracture (n=7/group) were dissected and fixed immediately in paraformaldehyde for 48 hours, followed by decalcification in 14% EDTA (pH 7.0) for 2 weeks. Samples were rinsed in PBS, infiltrated in 30% sucrose, and embedded in optimal cutting temperature compound (OCT compound, Tissue-Tek; VWR). A Cryojane Tape Transfer System (Leica) was used to create frozen longitudinal sections of the decalcified bone (Leica CM 1950 Manual Cryostat) at 5 µm thickness. Following sectioning, Click-iT EdU Alexa Fluor 647 Imaging Kit from ThermoFisher (C10340) was used to stain the sections for EdU and 4′,6-diamidino-2-phenylindole (DAPI; #D9542; 1:1000 dilution; Sigma-Aldrich, St. Louis, MO, USA). Briefly, frozen sections were thawed, washed with PBS, and permeabilized in 0.5% Triton X-100 (in PBS) for 20 min. The samples were then rinsed with PBS and incubated with 100 µL of the reaction cocktail (1x Click-iT reaction buffer, $CuSO_4$, 1x buffer additive, and Alexa Flour azide) for 30 min. Following additional rinsing in PBS, the slides were counterstained with DAPI. The whole femur was imaged using the Zeiss Axio Scan.Z1 slide scanner (20x objective) and images were assessed qualitatively for the presence of EdU-positive cells (pink).

Femurs designated for paraffin processing (n=4/group for EdU 3 week timepoint and n=7-8/group for 12 week timepoint) were dissected and fixed immediately in 10% neutral buffered formalin for 24 hours, followed by decalcification in 14% EDTA (pH 7.0) for 2 weeks. Standard paraffin processing was used such that fractured femurs were cut as longitudinal sections at a 5 µm thickness. Sections were stained with Picrosirius Red/Alcian Blue and the whole femur was imaged at 20x on a Nanozoomer slide scanner. Images were assessed qualitatively for callus composition and morphology.

The presence of osteoclasts was assessed using tartrate-resistant acid phosphatase (TRAP) staining on paraffin sections. Slides were manually evaluated to assess osteoclasts on the peripheral surface of the callus (osteoclast length/callus length (%)) and the percent of the callus surface occupied by cartilage, fibrous tissue, and bone was quantified. Note that for the 3 week animals, the periphery of the entire callus (top and bottom)

was analyzed for both WT and Col1-tk mice and varied in size, ranging from 4.8 to 14.8 mm. In 12 week animals, a 2 mm region spanning the original fracture site was analyzed for all mice due to the WT mice having healed by this timepoint.

Finally, a rat monoclonal endomucin antibody (clone eBioV.7C7, 1:400 dilution; eBiocience, Santa Clara, CA, USA) was used to note the presence of vessels at the callus site. Briefly, all paraffin slides were deparaffinized in xylene and rehydrated in graded ethanols. Proteinase K was used for antigen retrieval followed by processing as described in the Vectastain Elite ABC HRP kit (PK-6104; Vector Laboratories, Burlingame, CA, USA). ImmPact DAB peroxidase (HRP) substrate (SK-4105; Vector Laboratories) was used for detection and all slides were imaged at 20x on a Nanozoomer slide scanner. Note that an isotype control antibody (Clone eBR2a, 1:400 dilution; eBioscience) was used as a negative control. These slides were analyzed qualitatively due to the complexity of the vessels appearance throughout the callus.

Biomechanical Testing

Bilateral femurs were dissected at 12 weeks post fracture and cleaned of all soft tissue (n=6-9/group). The ends of each femur were potted using polymethylmethacrylate (PMMA, Ortho-Jet, Land Dental) in 6mm diameter x 12mm length acrylic tubes. The bone was centered using a custom fixture, leaving approximately 4.2 mm of exposed bone (including the callus region) between potting tubes. All samples were wrapped in PBS soaked gauze to preserve hydration while the PMMA cured overnight. The following day, each sample was loaded into a custom-built torsion machine with a 25 in-oz load cell controlled with LabVIEW software (LabVIEW 2014, National Instrument, TX). The machine held one of the potted femur ends in a fixed position while rotating the other potted tube at 1 deg/sec until fracture. The maximum torque (Nmm), rotation at maximum torque (degrees), and stiffness (Nmm/degree) were calculated from the resulting torque-rotation graphs (Matlab).

Statistics

Prior to experiments, study sample sizes were calculated based on a power analysis with $\alpha = 0.05$ and $\beta = 0.20$ (https://www.stat.ubc.ca/~rollin/stats/ssize/n2.html). Estimates of sample variance and effect size were based on previous experimental data and biological importance. Target samples sizes for outcomes per experimental group were: MicroCT: n = 8, Histology: n = 7, Biomechanics: n = 10. Actual sample sizes are noted above and in Results. A chi-square test was used to assess fracture union based on the Goldberg scale for each timepoint. An unpaired t-test was used to compare WT and Col1-tk microCT data taken at 3 weeks after fracture. TRAP histological quantification taken at 3 and 12 weeks post fracture was also analyzed using an unpaired t-test. Two-way ANOVA with Sidak's post hoc test to correct for multiple comparisons was used for *in-vivo* microCT (repeated factor: *time*; between factor: *genotype*). *Ex-vivo* microCT and torsion testing data were also analyzed using two-way ANOVA with Sidak's post hoc test (repeated factor: *side* [intact, fractured];

between factor: *genotype*). Significance was considered at p values < 0.05. All data analysis was performed using Prism (Version 8; GraphPad Software, La Jolla, CA, USA).

Results

Bone Bridging and Callus Formation in Col1-tk Mice is Greatly Reduced at 3 Weeks.

To first confirm targeting of tk+ cells with GCV, HSV-tk expression was evaluated in fracture callus at 2 weeks post fracture. WT mice given GCV displayed typical callus composition with both woven bone and cartilage, but no tk+ staining (**Supplementary Figure 1A, A'**). In Col1-tk mice dosed with vehicle (H_2O), callus composition appeared normal and tk+ expression was noted in cells within the woven bone and cartilage regions (**Supplementary Figure 1B, B'**). However, in Col1-tk mice dosed with GCV, the fracture callus was reduced in size and lacked both woven bone and cartilage; some tk+ cells were present in the expanded periosteum (**Supplementary Figure 1C, C'**).

Healing was evaluated by weekly radiographs which were blindly scored using a modified Goldberg score (**Figure 2A**). At 1 week after fracture, almost no bridging had occurred in either genotype. At 2 weeks, over 80% of the WT mice had at least one side bridged, compared to just over 50% of Col1-tk mice. After 3 weeks, there was some bridging in 100% of WT mice, and 83% had complete bridging; this was significantly different than Col1-tk mice, where there was some bridging in 77% of samples, but no samples were completely bridged, and 23% remained unbridged (χ^2, $p < 0.0001$). Representative radiographic images demonstrate good and poor healing outcomes in WT and Col1-tk mice, respectively (**Figure 2B**). Additionally, 3D reconstructions of *ex vivo* microCT scans show a robust callus formed at the fracture site of WT femurs while the Col1-tk femurs showed greatly reduced callus formation (**Figure 2B**). Quantitative analysis of these scans demonstrate an approximate 50% reduction in BV and TV from WT to Col1-tk ($p < 0.001$; **Figure 2C**). Measures of density, i.e., vBMD and TMD, were greater in Col1-tk compared to WT femurs ($p < 0.05$), reflecting a larger relative contribution of the original (dense) cortical bone to the total bone within the ROI. In addition, the BV, TV, vBMD, and TMD values for Col1-tk were closer to average values for the intact femurs (dashed line).

To further analyze healing, histological evaluation was completed using Picrosirius Red/Alcian Blue and EdU/DAPI staining (**Figure 3**). The WT femurs appeared fully (or nearly fully) bridged by a large woven bone callus, with only a small amount of cartilage (**Figure 3A, A'**). Bright EdU+ cells can be seen within representative fracture callus, indicating a localized increase in proliferation (**Figure 3B, B'**). In comparison, the Col1-tk femurs only formed a small callus, with less bone and more cartilage and fibrous tissues than WT (**Figure 3C, C'**). Col1-tk femurs had fewer EdU+ cells (**Figure 3D, D'**). A subset of fractured Col1-tk mice were given either EdU or both EdU/GCV for 1 week (**Supplementary Figure 2**). Col1-tk mice given only EdU displayed a typical fracture callus with EdU+ proliferative cells throughout (**Supplementary Figure 2A, B**).

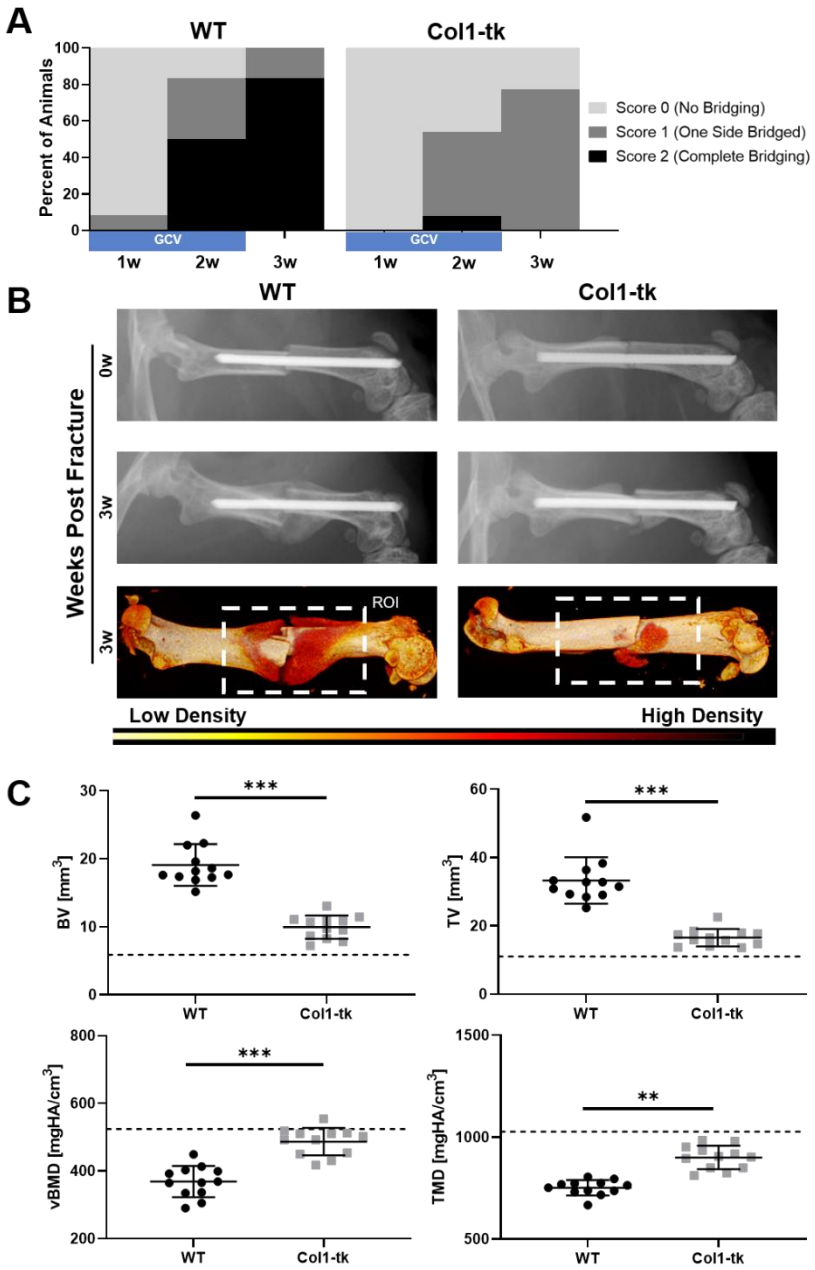

Figure 2. Following fracture, early healing was evaluated by weekly X-rays as well as *ex vivo* microCT. (A) Bridging evaluated by a modified Goldberg scale demonstrated the progression of callus bridging in WT mice as compared to reduced or absent bridging in Col1-tk mice. (B) This lack of bridging and reduced callus formation in Col1-tk mice can also be visualized in both radiographic images and microCT 3D reconstructions (ROI = 6.3 mm region of interest for microCT analysis includes cortical bone and callus). (C) MicroCT quantification showed significantly less BV and TV in Col1-tk vs. WT mice, but significantly higher vBMD and TMD (**$p < 0.01$, ***$p < 0.001$). Average values of BV, TV, vBMD, and TMD for intact femurs are noted by a dashed line.

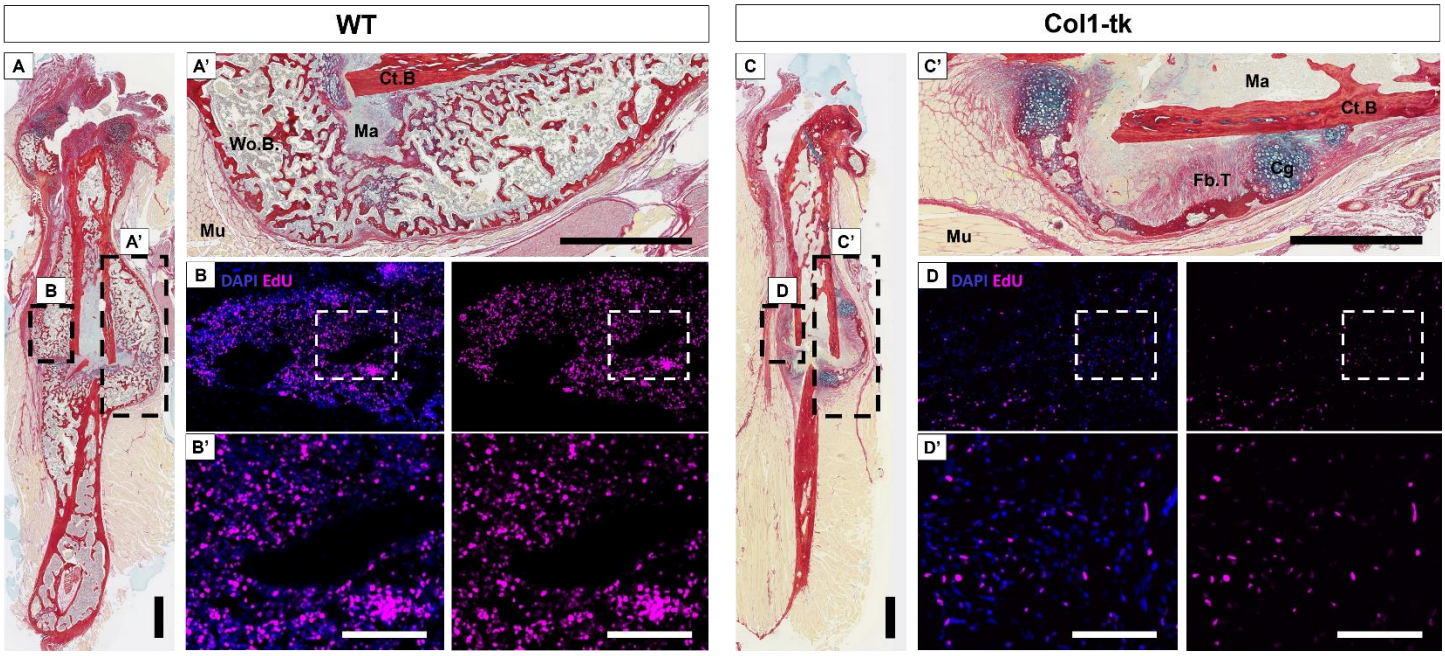

Figure 3. Healing at 3 weeks post fracture was qualitatively assessed using histological staining with either Picrosirius Red/Alcian Blue or EdU(pink)/DAPI(blue). (A, A') Sagittal sections from the fracture midpoint of WT mice had complete bridging with the callus almost entirely composed of woven bone (Wo.B; red stain). (B, B') There was abundant proliferation within the fracture callus as shown by the EdU stain in a representative cross-section. (C, C') The Col1-tk sections had a smaller callus composed of mostly cartilage (Cg; blue stain) and fibrous tissue (Fb.T), with little woven bone. (D, D') While proliferation is present at the callus site of Col1-tk femurs, it is greatly reduced in both quantity and intensity as shown in a representative cross-section. Abbreviations: Cortical Bone = Ct.B,; Cartilage = Cg; Fibrous Tissue = Fb.T.; Marrow = Ma; Muscle = Mu; Woven Bone = Wo.B. Black and white scale bars denote 1 mm and 100 µm, respectively.

Similarly, while Col1-tk mice treated with both EdU and GCV displayed a smaller callus at the fracture site, there was still evidence of EdU+ cells (**Supplementary Figure 2C, D**).

TRAP and endomucin staining were performed to assess the presence of osteoclasts and vasculature, respectively (**Figure 4**). WT mice displayed an abundance of TRAP+ woven-bone lining osteoclasts along the callus surface (**Figure 4A, A', A"**). While the Col1-tk mice also had osteoclasts lining some woven bone (**Figure 4B, B"**), this was not seen consistently throughout the callus (**Figure 4B'**). Over 90% of the WT callus periphery was composed of bone, whereas the Col1-tk callus surface was only about 20% bone, with the remaining 57% and 23% consisting of fibrous tissue and cartilage, respectively (**Figure 4C**). Osteoclast length per callus length was significantly greater in WT compared to Col1-tk mice (22% vs. 0.8%, $p < 0.001$; **Figure 4D**). Endomucin staining revealed a large amount of vasculature throughout the entire callus in the WT mice (**Figure 4E, F**). Comparatively, while the Col1-tk mice had some vasculature (**Figure 4H**), a majority of the fracture site displayed little to no endomucin staining (**Figure 4G**).

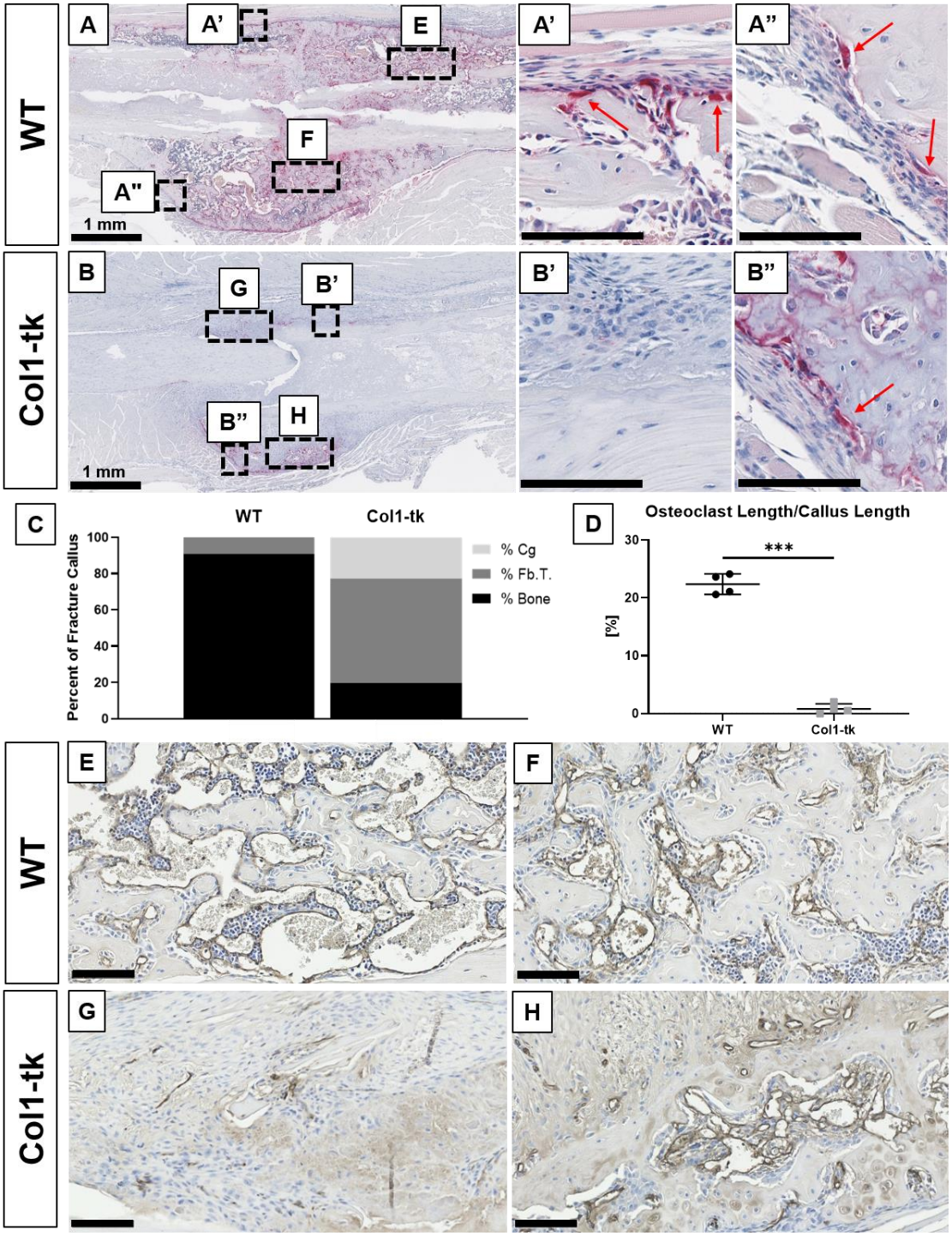

Figure 4. Osteoclast (TRAP+) activity and the presence of vessels was evaluated in WT and Col1-tk mice at 3 weeks post fracture. (A) WT mice displayed a large amount of (red) TRAP+ osteoclasts lining the woven bone along the callus surface, noted by red arrows (A', A"). (B) The Col1-tk mice also had osteoclasts lining some woven bone, but this was greatly reduced (B', B"). (C) The callus surface of WT mice was primarily composed of bone and (D) the ratio of the length of osteoclasts to woven bone was significantly higher as compared to Col1-tk mice (***$p < 0.001$). The Col1-tk callus surface was largely composed of fibrous tissue (Fb.T) and cartilage (Cg), in addition to bone. (E, F) Endomucin staining (brown) of the vessels was very prevalent throughout the callus of WT mice. (G, H) Comparatively, the Col1-tk mice had some staining, but overall reduced vasculature. Black scale bars denote 100 μm unless otherwise noted.

Radiographic Healing is Impaired in Col1-tk Mice 12 Weeks Post Fracture.

To evaluate the effects of transient ablation of proliferating osteoblasts on long-term fracture healing, WT and Col1-tk mice were dosed with GCV for 2 or 4 weeks, the drug withdrawn, and the progression of healing followed until sacrifice at 12 weeks. WT mice, dosed for either 2 or 4 weeks, displayed a large callus formed around the fracture site at 2 weeks and this callus condensed over time (**Figure 5**). Based on the blinded scoring, nearly all WT fractures had fully bridged after 4 weeks of healing. In comparison, while the Col1-tk mice also developed a callus, it was greatly reduced in size compared to WT mice and remained this way over 12 weeks. Any small mineralized callus present was visible by week 4 and remained consistent in size thereafter. For the Col1-tk mice dosed with GCV for 2 weeks (**Figure 5A**), between 5 and 12 weeks after fracture only 20 - 65% of femurs appeared fully bridged. Similarly in the Col1-tk mice dosed with GCV for 4 weeks (**Figure 5B**), only 10 – 50% of femurs appeared fully bridged in the 5 to 12 weeks after fracture. The radiographic scores of WT and Col1-tk mice were significantly different from one another at all timepoints beginning at 2 weeks post fracture (2w GCV: χ^2, $p < 0.05$; and 4w GCV: χ^2, $p < 0.01$).

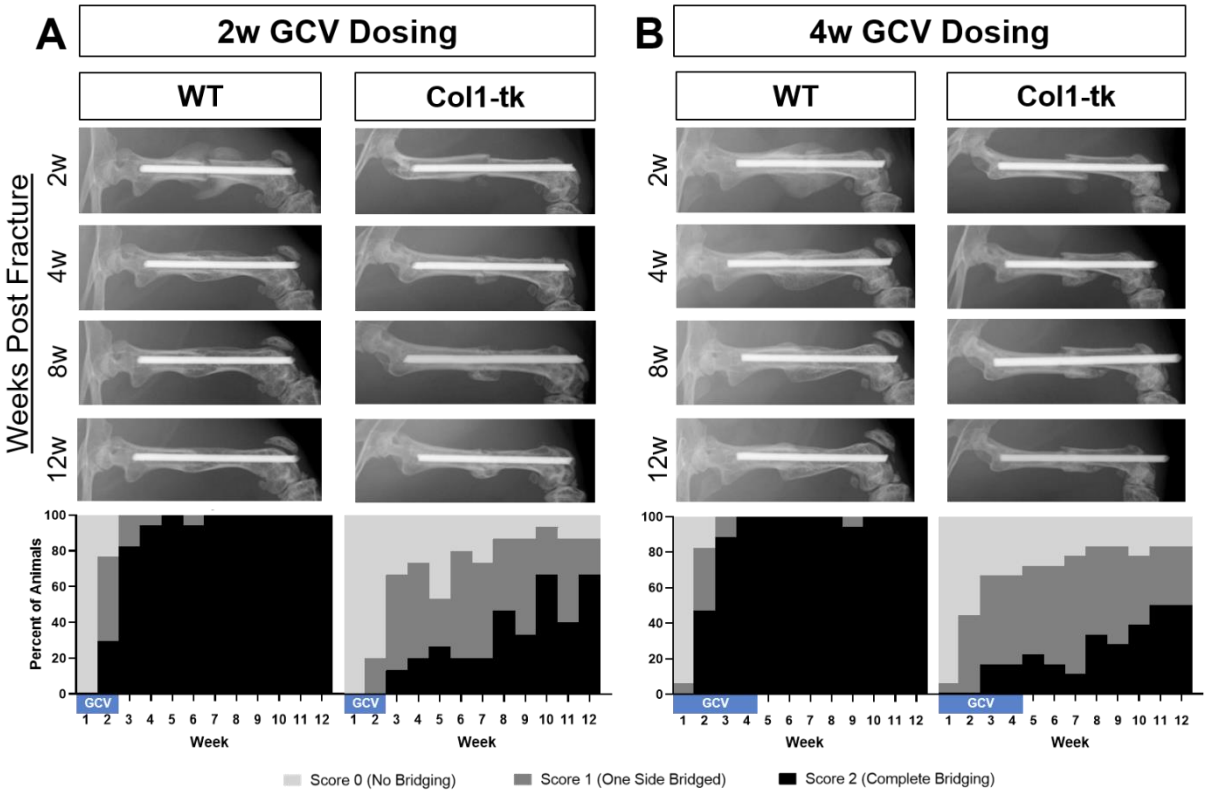

Figure 5. Radiographs were taken weekly following fracture until euthanasia at week 12. Representative X-rays are shown at 2, 4, 8, and 12 weeks for both WT and Col1-tk mice dosed with GCV for either (A) 2 or (B) 4 weeks immediately following fracture. Scoring was completed using a modified Goldberg scale. WT mice, regardless of dosing scheme, were fully bridged 4 weeks after fracture. By the end of the study only half of the Col1-tk fractures appeared completely bridged. Scoring of the radiographs demonstrated a significant difference between WT and Col1-tk mice with both 2w ($\chi 2$, $p < 0.05$) and 4w dosing ($\chi 2$, $p < 0.01$).

In Vivo MicroCT Shows Small Initial Callus Volume that Does Not Change over 12 Weeks in Col1-tk Mice.

To further track the healing progression through 12 weeks, *in vivo* microCT scans were taken at 2 to 4 week intervals (**Figure 6**). Of the mice dosed with GCV for 2w, WT mice had a significantly larger callus volume and length at all timepoints as compared to the Col1-tk mice (**Figure 6A**; $p < 0.05$). In the 4w GCV treated group, WT mice had a larger, longer callus compared to Col1-tk mice at 4 weeks post fracture (**Figure 6B**; $p < 0.001$). Callus size in WT mice was greatest at 2 weeks and then reduced progressively with time, whereas the Col1-tk callus volume and length, for both dosing schemes, did not significantly change over time.

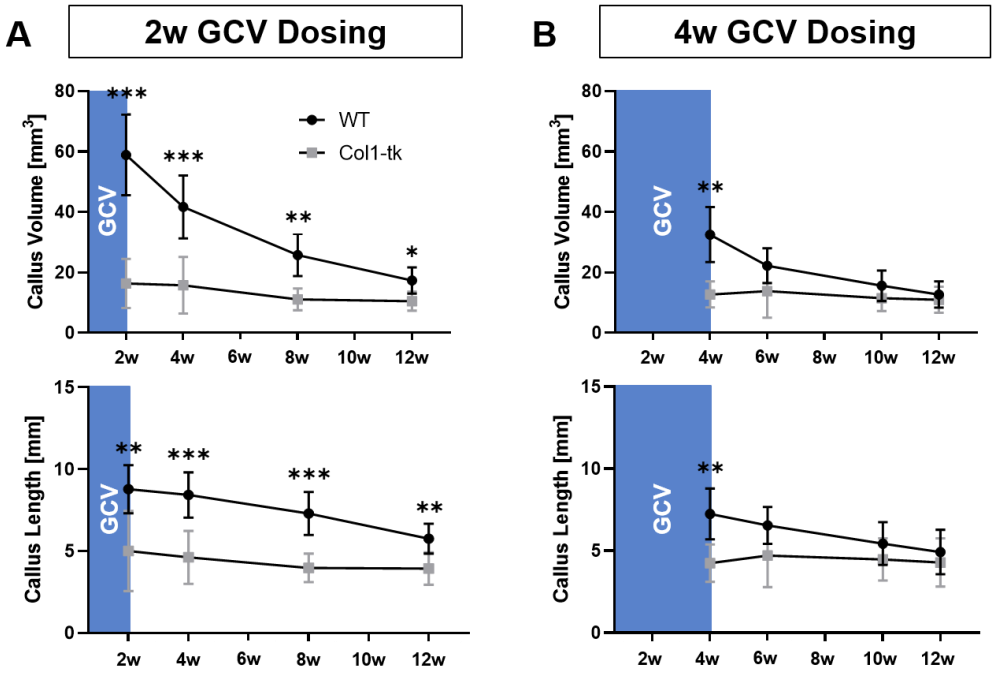

Figure 6. *In vivo* microCT was used to evaluate both callus volume (mm^3) and length (mm) throughout the 12 weeks of fracture healing. (A) Following 2w of GCV dosing, both WT callus volume and length were significantly larger than that of Col1-tk at 2, 4, 8, and 12 weeks. (B) 4w GCV dosing resulted in a significant difference between WT and Col1-tk callus volume and length at the 4 week timepoint. Notably, while WT calluses reduced volume and length over time, there was no significant change in Col1-tk callus size, for either dosing scheme, over time (*$p < 0.05$, ** $p < 0.01$, ***$p < 0.001$).

Ex Vivo MicroCT and Histology Show Lack of Bridging 12 Weeks Post Fracture in Col1-tk Mice.

After 12 weeks of healing, animals were euthanized and both femurs dissected for microCT analysis (**Figure 7**). In WT mice, regardless of dosing scheme, the fracture site was completely bridged by a thin outer cortical shell at the margin of a consolidated callus, and a second inner cortex of similar outer diameter as the original cortex. There were no visible fracture surfaces. Calluses in the WT mice had similar BV as intact bones, but significantly greater TV (**Figure 7A, 7B**), indicating comparable bone mass distributed over a larger volume. Consequently, WT calluses had reduced vBMD and TMD compared to intact femur for both dosing schemes ($p < 0.001$). By contrast, in Col1-tk mice much of the original cortical bone was still fragmented, with visible

fracture surfaces and lack of bridging (**Figure 7A, 7B**). The callus region in Col1-tk mice had significantly greater BV and TV compared to the intact femur for both dosing schemes ($p < 0.01$), indicating greater bone mass that was distributed over a larger volume. Consequently, the fractured Col1-tk femurs had similar vBMD as intact bone.

Histological sections at the fracture site at 12 weeks were stained and imaged (**Figure 8**). All WT femurs had complete bridging with continuous cortical bone; there was no cartilage or fibrous tissue and the original fracture surfaces were not obvious. The thin outer and inner cortices seen on microCT were also evident as collagen-rich, aligned bone tissue. In contrast, the Col1-tk femurs all had clearly evident fracture surfaces, with regions that looked like original cortical bone. Col1-tk femurs had some calcified areas on the outside of the callus, and also had varying degrees of cartilage and fibrous tissue, demonstrating incomplete endochondral bone formation. When stained for TRAP+ osteoclasts, both the WT and Col1-tk callus periphery had some positive staining (**Supplementary Figure 3A, A', A", B, B', B"**). The periphery of the callus of both WT and Col1-tk mice was primarily composed of bone (100% in WT and 72% in Col1-tk), but the Col1-tk fracture site also had fibrous tissue (**Supplementary Figure 3C**). Quantitative analysis of osteoclast length per callus length revealed fewer osteoclasts covering the WT callus than at 3 weeks (**Figure 4**), although still significantly more than Col1-tk ($p < 0.05$; **Supplementary Figure 3D**). Endomucin staining revealed almost no vessels at the original site of fracture in WT mice (**Supplementary Figure 3E, F**) and minimal vasculature in Col1-tk mice (**Supplementary Figure 3G, H**).

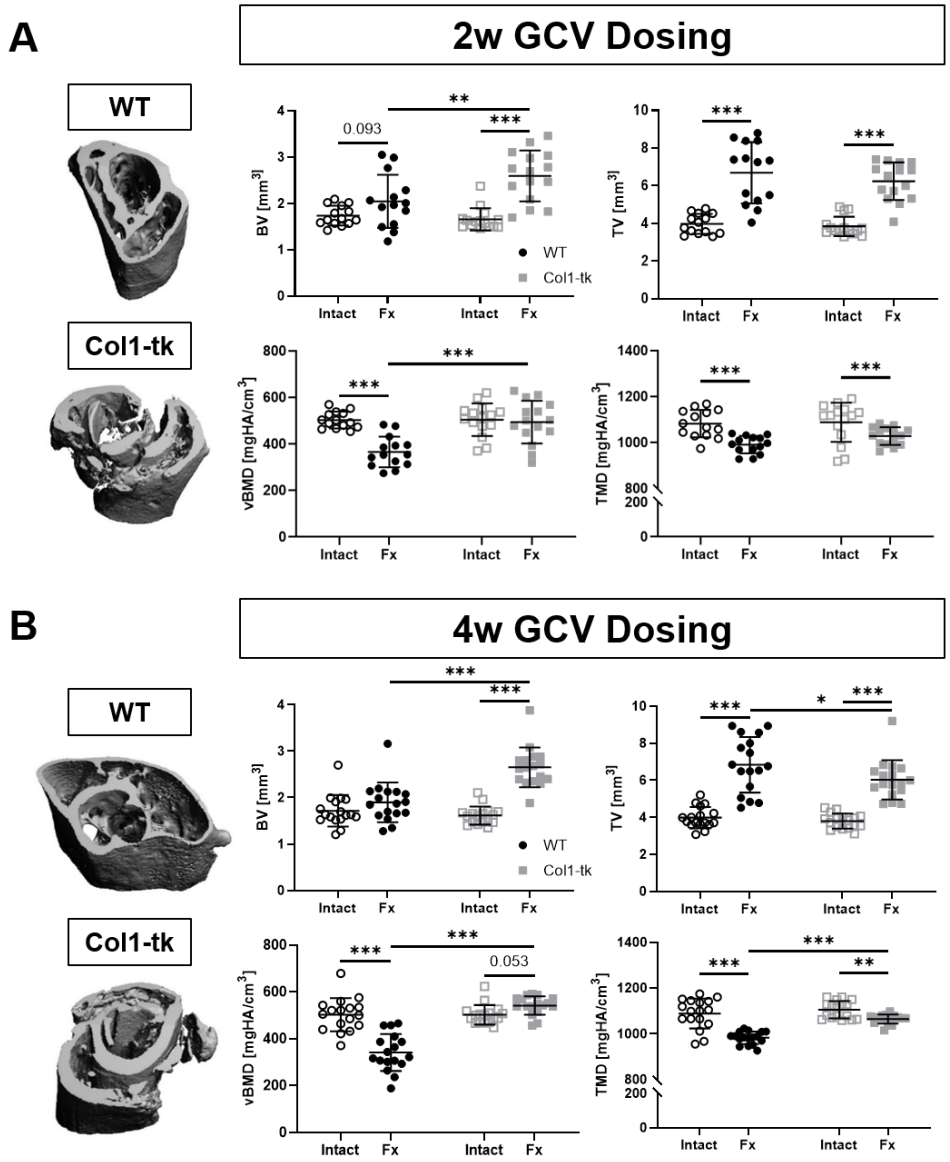

Figure 7. *Ex-vivo* microCT data for WT and Col1-tk intact and fractured (Fx) femurs for both (A) 2 and (B) 4w GCV dosing. Representative micro-CT 3D reconstructions displayed a thin, contiguous outer cortex integrated with an inner cortex in WT mice for both dosing schemes. In comparison, the Col1-tk reconstructions show evident of the original cortical bone with poor consolidation and incomplete bridging at the callus site. (A) For 2w GCV, WT mice had significantly different TV, vBMD, and TMD between intact and Fx femurs. Col1-tk had significantly different BV, TV, and TMD between intact and Fx femurs. (B) Similarly, 4w GCV also resulted in significantly different TV, vBMD, and TMD between the WT intact and Fx femurs. The Col1-tk mice also had significantly different BV, TV, and TMD between the intact and Fx femurs. Finally, the WT and Col1-tk Fx femurs had significantly different BV and vBMD for 2w GCV dosing and BV, TV, BMD, and TMD for 4w GCV dosing (*$p < 0.05$, ** $p < 0.01$, ***$p < 0.001$).

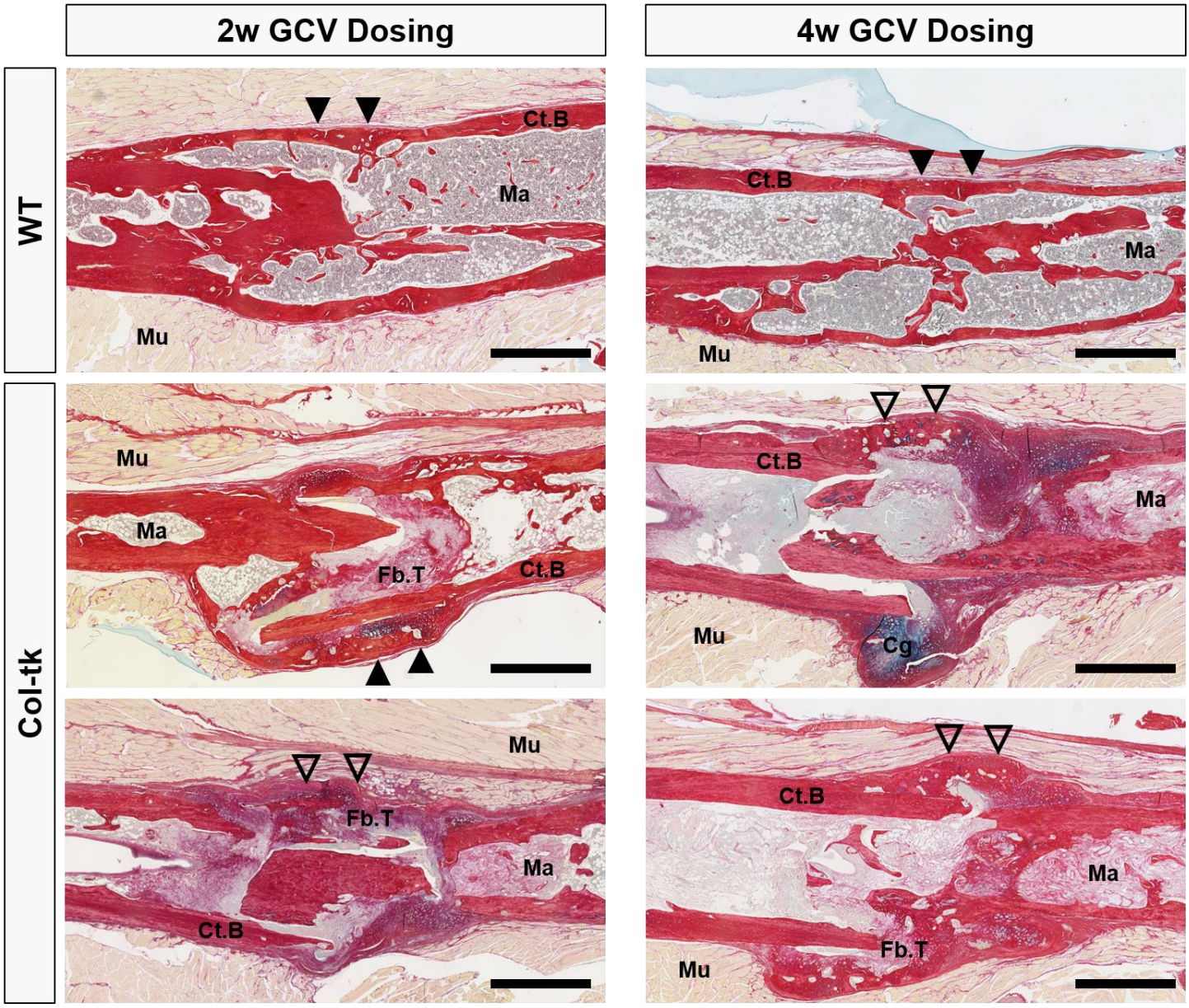

Figure 8. Representative Picrosirius Red/Alcian Blue staining of the WT and Col1-tk fracture site at 12 weeks post fracture. Regardless of GCV dosing timeline (2 or 4 week), WT mice had consistent, complete bridging by 12 weeks as shown by contiguous cortical bone (bright red staining; filled arrowheads), with little evidence of the original fracture site. The Col1-tk femur calluses had variable healing at 12 weeks (shown by two examples for each dosing group). The callus had some cortical bridging (filled arrowheads) in addition to pockets of woven bone at a still visible fracture site (open arrowheads). The Col1-tk fracture sites had some persistent cartilage and fibrous tissue. Abbreviations: Cortical Bone = Ct.B,; Cartilage = Cg; Fibrous Tissue = Fb.T.; Marrow = Ma; Muscle = Mu. Black scale bars denote 1 mm.

Col1-tk Mice Have Inferior Torsional Properties at 12 Weeks Post Fracture.

To assess whether a functional union was achieved, torsional testing was completed on both intact and fractured ("healed") femurs from WT and Col1-tk mice (**Figure 9**). All intact femurs failed by spiral fracture within 10 degrees of rotation. In WT mice, the maximum torque and rotation at maximum torque of fractured femurs were not significantly different from intact femurs, indicating return to normal function. The only evidence of incomplete recovery in fracture femurs of WT mice was lower than normal stiffness in the 2w (but not 4w) GCV group. In stark contrast, the fractured femurs in Col1-tk mice had significantly reduced stiffness and increased rotation at maximum torque compared to intact femurs for both dosing groups, and decreased maximum torque in the 2w GCV group. Moreover, comparing fractured femurs between genotypes, Col1-tk femurs had significantly lower stiffness and greater rotation at maximum torque for both dosing timelines, indicating more compliant and less stable behavior, and maximum torque was significantly lower for the 4w GCV group, indicating inferior strength.

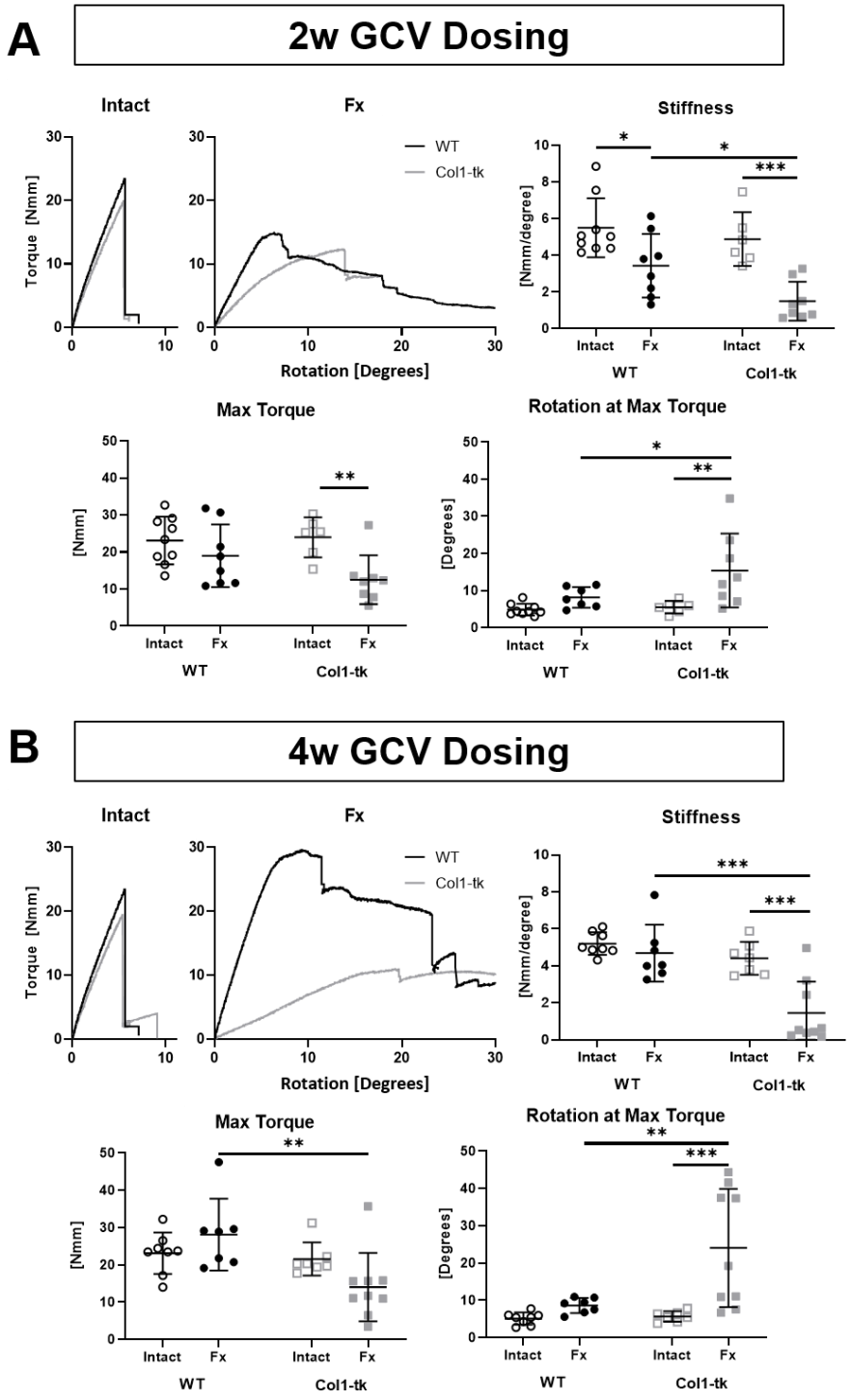

Figure 9. Biomechanical testing was completed to assess fracture stability and strength for (A) 2w and (B) 4w GCV dosed intact and fractures (Fx) femurs. Representative torque-displacement curves are shown. Regardless of dosing scheme, intact femurs failed before reaching a rotation of 10 degrees. (A) In WT mice, 2w GCV intact and Fx femurs had significantly different stiffness. In Col1-tk, 2w GCV, stiffness, maximum torque, and rotation at maximum torque were all significantly different between intact and Fx femurs. (B) For the Col1-tk, 4w GCV, the stiffness and rotation at maximum torque were significantly different between intact and Fx femurs. Comparisons of Fx femurs between genotypes noted significant differences in stiffness and rotation at maximum torque for both GCV dosing timelines (*$p < 0.05$, ** $p < 0.01$, ***$p < 0.001$).

Discussion

Our work with the Col1-tk model has allowed us to create a novel murine model of atrophic nonunion. The failure of bone to heal, defined as fracture nonunion, is a common clinical complication with substantial healthcare burden. Models of atrophic nonunion have been around as early as 1999, providing an *in vivo* representation of the bone's inability to heal, resulting in nonunion [6, 8]. Animal models of atrophic nonunion have focused on fractures that will not heal over the animal's lifetime, typically induced mechanically or physically. While many early studies created these models of atrophic nonunion in rabbits [30-32], more recent work has migrated towards rat [33-37] and mouse [13] models. Specifically, a recent study by Wang, L., et al. [38] demonstrated a nonsurgical atrophic nonunion fracture model using radiation to induce periosteal damage. As fracture is a late side effect of radiation therapy, this model provides an appropriate model of the delayed healing response that is clinically difficult to treat. However, while these approaches result in atrophic nonunion, such invasive methods are not always representative of clinical nonunions where osseous regeneration has been arrested by a disturbance of metabolic pathways [1, 9]. Thus, there remains a need for the development of a more relevant, pre-clinical atrophic nonunion model to test therapeutic interventions. While previous work has studied the proliferative response following fracture, the cells contributing to this have not clearly been identified. Instead, the progression of these cells between the cartilage, fibrous tissue, and newly formed bone has been noted throughout the healing process [17-19]. Previous work has demonstrated the use of Col1a1 promoters to distinguish between the various stages of osteoblast differentiation [21]. Specifically, the Col3.6 promoter is expressed in preosteoblasts, whereas the Col2.3 promotor marks those cells later in the osteoblast lineage. Due to the known expression of 3.6Col1a1 in periosteal (osteoblast lineage) cells and their role in bone formation, it is of interest to block 3.6Col1a1 proliferation following fracture to note the role in healing [21, 22]. Transgenic 3.6Col1A1-tk (Col1-tk) mice provide a tool to target replicating osteoblast progenitors and subsequently ablate them with the addition of ganciclovir (GCV) drug [24]. Therefore, the central hypothesis of this project was that the Col1-tk mouse provides a unique model of atrophic nonunion, through the inability to form an osteochondral periosteal callus. A 2 or 4 week suppression of osteoblast proliferation following fracture resulted in limited callus formation. Specifically, Col1-tk calluses had over 50% less volume at two weeks post fracture, and over time volume or composition did not change resulting in a functionally weaker bones at 12 weeks. These deficiencies in healing suggest that osteoblast proliferation within the first two weeks of fracture healing is critical to successful bone union.

While it is known that cell proliferation occurs during fracture healing, the importance of osteoprogenitor cell proliferation has not been directly tested [14, 17, 18, 39]. Using the Col1-tk mouse, we demonstrated that blocking proliferation in the first two weeks is critically important to callus formation. We dosed mice with GCV for 2 weeks following fracture, to target the proliferative phase of healing. It was anticipated that if the Col1-tk mouse was able to recover from the 2w GCV dosing, withdrawal of the drug would result in a peak in proliferation at the 3 week timepoint as it would emulate what would be 1 week post fracture. While all WT mice displayed complete bridging, the Col1-tk mice developed a significantly smaller and less mature callus **(Figures 2** and **3**). Interestingly vBMD and TMD were significantly larger in the Col1-tk mice at 3 weeks. It is

our interpretation that vBMD is higher in Col1-tk femurs due to the substantially lower total volume within the analysis region. Increases in TMD reflect the lack of new bone formation, as the larger proportion of mineralized bone included in the measurement is from the original (highly dense) cortex. These first results indicated that arresting osteoblast proliferation during the first two weeks of healing is a significant detriment to healing. Despite the initial EdU+ proliferative response seen at 1 week following fracture in both WT and Col1-tk mice (**Supplementary Figure 2**), proliferation was overall substantially impacted in Col1-tk mice. A large number of EdU+ cells were present within the fracture callus of the WT animals, demonstrating proliferation of many cell types occurring following fracture. While the Col1-tk mice had some proliferation within their reduced callus, it was greatly reduced in scale (**Figure 3**). The periosteum and mesenchymal stem cell proliferation are primary cell sources for fracture healing [14, 40]. However, studies have also shown that muscle stem cells contribute to the callus, suggesting a source of this initial proliferation. It is also possible that the Col1-tk proliferation is stemming specially from the endochondral ossification (secondary healing) process [39]. Compositionally, the WT callus surface had a significantly higher content of osteoclasts and bone as compared to the Col1-tk mice whose callus also contained high percentages of fibrous tissue and cartilage. This further supports the lack of remodeling occurring in the Col1-tk callus as compared to the normal healing in WT mice. Additionally, there was extensive vasculature throughout the callus of the WT mice which is essential in early stages of fracture healing [41]. However, vasculature was reduced at the fracture site of the Col1-tk mice which could impact the healing response (**Figure 4**). Overall, the Col1-tk mice could not fully recover from the dosing induced ablation of proliferating osteoprogenitor cells during the peak fracture healing timeline.

We next demonstrated that preventing early cell proliferation leads to a functional nonunion evaluated at 12 weeks. The fractured WT mice healed as previously shown in literature where a callus was formed, remodeling occurred, and the bone was resorbed back to the original femur structure [13, 42, 43]. In contrast, when the Col1-tk mice were fractured a reduced callus was formed, but most of the fractured cortical bone was pushed together and never underwent full remodeling. Thus, the Col1-tk mice contain a higher percentage of original, dense cortical bone than the remodeling WT mice and thus, have a higher BV and BMD. The 3D reconstructions (**Figure 7**) visually depict this with thin cortical bone of the newly healed WT mice as compared to the fractured Col1-tk mice which still possessed much of the original cortical bone from the time of fracture. This is further illustrated with histological sections and, in addition to the bridging noted above, there was a high content of fibrous tissue and cartilage further demonstrating that the fractured Col1-tk mice were not able to recover from the dosing induced nonunion (**Figure 8**). Both the WT and Col1-tk mice displayed essentially no TRAP+ woven bone lining osteoclast activity and reduced vasculature demonstrating both completed healing and halted healing, respectively (**Supplementary Figure 3**). Notably, there was no significant different in overall callus size, number of osteoclasts, or total osteoclast length (as compared to the entire callus) between Col1-tk mice at 3 weeks and 12 weeks post fracture. This further demonstrates Col1-tk lack of progression in the healing response, even following the long-term withdrawal of GCV. Finally, when the femurs were biomechanically tested, the Col1-tk mice were significantly weaker than the WT mice (**Figure 9**). These results support the Col1-tk mouse as a function nonunion; however atrophic nonunions are characterized by a reduced callus and fibrous tissue formation throughout the fracture site [10]. The fractured Col1-tk mouse

presented aspects both in favor and against its use as a model of atrophic nonunion. Specifically, while the Col1-tk mouse does have some callus formation and bridging, making it an imperfect model of atrophic nonunion, the lack of healing, high content of fibrous tissue, and biomechanical instability support it as an acceptable model based on the clinical definitions of a nonunion.

The Col1-tk mice in this experiment were dosed for both 2 and 4 weeks to identify the ideal dosing window to create a permanent nonunion. The results of the two dosing schemes were arguably very similar. While 4w GCV resulted in less bridging radiographically (**Figure 5**), 2w GCV had a larger significant difference between the WT and Col1-tk callus size/length *in vivo* (**Figure 6**). 4w GCV dosing resulted in slightly larger differences in *ex vivo* microCT between both WT and Col1-tk fractured femurs, as well as Col1-tk intact vs. fractured femurs (**Figure 7**). However, both dosing schemes resulted in fracture sites filled with fibrous tissue and cartilage that were indistinguishable histologically and biomechanically **(Figure 8** and **9**). Overall, both dosing schemes led to a dosing induced nonunion and thus, 2w GCV should provide sufficient dosing for future work. As 4w GCV spanned the entire typical fracture healing timeline, it was unexpected that it did not have a more permanent effect on the healing process than the shorter 2w GCV [10, 13]. These results demonstrate that arresting osteoblast proliferation during the first two weeks of healing is a significant detriment to healing and further establishes how essential the healing process during those first two weeks is to a full recovery.

There were several limitations to the successful use of this model, as well as suggestions for future studies. Due to the ability of the 2w GCV dosing scheme to prevent recovery from the fracture and subsequent development of a nonunion, it is of interest to explore shorter windows of proliferative ablation. A shorter dosing scheme could be used to further examine the potential rescue of the callus. Additionally, the dosing start time could be delayed to note at what point the fracture healing progression has gained enough momentum to not be affected by this proliferation ablation. This model used an intramedullary pin for fracture stabilization. Other options include intramedullary locking nail or compression screw, external fixator, a pin-clip device, and locking plates [44]. It is important to consider potential stress shielding with various models as it can cause asymmetric callus formation or even prevent a periosteal response [45]. It would also be of interest to vary the fracture model by both type and location. While the femur and tibia are accepted as appropriate bones for studying fracture healing, others such as the ulna, rib, radius, and mandible could be useful alternatives [44]. In addition, the full fracture model from this study utilizes both intramembranous and endochondral healing [26, 27]. To further identify the role of ablating proliferation in the healing process, a stress fracture model could also be used to focus primarily on intramembranous ossification [46, 47].

In conclusion, we have successfully developed a novel murine model of atrophic nonunion. We utilized a Col1-tk mouse model that showed an incomplete fracture and reduced osteoblast proliferation, normally an important step in fracture healing. In addition, the Col1-tk mice were shown radiographically and biomechanically to have a functional nonunion. The necessity for such a study is supported by the clinical prevalence of atrophic nonunion combined with the expressed need for a clinically relevant model to further study the biology of such a complex nonunion. This work will impact the field of orthopaedic surgery, specifically the ability to better understand atrophic nonunion and improve intervention techniques for appropriate clinical treatment.

Acknowledgements:

This work was supported by funding from NIAMS (R01 AR050211, P30 AR057235, R21 AR076636-01, T32 AR060719, and F32 AR076191-01). The authors would like to thank the Washington University in St. Louis Musculoskeletal Research Center (MRC) Cores and staff for assistance. Specifically, thanks to Yung Kim for all X-ray and microCT (Scanco) acquisition assistance. Also thanks to both Crystal Idleburg and Samantha Coleman for histological processing and sectioning of all specimens. Thanks also to Dennis Oakley of the Washington University in St. Louis Center for Cellular Imaging (WUCCI) Core and Heather Zannit for training and frozen section imaging assistance. Paraffin histological images were taken with the Nanozoomer at Alafi Neuroimaging Core (S10 RR027552). Thank you to Nicole Migotsky for torsion testing and LabVIEW software instruction. Finally, thank you to Evan G Buettmann for initial animal training and handling training, as well as pilot work. 3.6Col1a1-tk mice were kindly provided by the labs of Drs. Robert Jilka and Charles O'Brien (University of Arkansas for Medical Sciences, Little Rock, AR, USA).

Authors' Roles: Study design: KRH, JAM, MJS. Study conduct: KRH, DAWS, SY, AH, DS, JAM. Data collection: KRH, DAWS, SY, DS, JAM. Data analysis: KRH, DAWS, SY, AH, JAM. Data interpretation: KRH, JAM, ANM, MJS. Drafting manuscript: KRH. Revising manuscript: KRH, JAM, MJS. Approving final version of manuscript: KRH, JAM, MJS. KRH takes responsibility for integrity of data analysis.

References:

1. Choi, P., et al., *Cellular and molecular characterization of a murine non-union model.* Journal of Orthopaedic Research, 2004. **22**(5): p. 1100-1107.
2. Nandra, R., L. Grover, and K. Porter, *Fracture non-union epidemiology and treatment.* Trauma, 2016. **18**(1): p. 3-11.
3. Einhorn, T.A., *Enhancement of fracture-healing.* J Bone Joint Surg Am, 1995. **77**(6): p. 940-56.
4. Cadet, E.R., et al., *Proximal humerus and humeral shaft nonunions.* J Am Acad Orthop Surg, 2013. **21**(9): p. 538-47.
5. Mills, L.A. and A.H. Simpson, *The relative incidence of fracture non-union in the Scottish population (5.17 million): a 5-year epidemiological study.* BMJ Open, 2013. **3**(2).
6. Mills, L.A. and A.H. Simpson, *In vivo models of bone repair.* J Bone Joint Surg Br, 2012. **94**(7): p. 865-74.
7. Miclau, T., in *Intl Society for Fracture Repair*. 2018: New Orleans.
8. Boyan, B.D., et al., *Osteochondral progenitor cells in acute and chronic canine nonunions.* J Orthop Res, 1999. **17**(2): p. 246-55.
9. Markel, M.D., et al., *Atrophic nonunion can be predicted with dual energy x-ray absorptiometry in a canine ostectomy model.* J Orthop Res, 1995. **13**(6): p. 869-75.
10. Garcia, P., et al., *Rodent animal models of delayed bone healing and non-union formation: a comprehensive review.* Eur Cell Mater, 2013. **26**: p. 1-12; discussion 12-4.
11. Liu, X., et al., *Exogenous hedgehog antagonist delays but does not prevent fracture healing in young mice.* Bone, 2017. **103**: p. 241-251.
12. Morshed, S., *Current Options for Determining Fracture Union.* Advances in medicine, 2014. **2014**: p. 708574-708574.
13. Garcia, P., et al., *Development of a reliable non-union model in mice.* J Surg Res, 2008. **147**(1): p. 84-91.
14. Zuscik, M.J., *Skeletal Healing*, in *Primer on the Metabolic Bone Diseases and Disorders of Mineral Metabolism*, C.J. Rosen, Editor. 2013.
15. Colnot, C., X. Zhang, and M.L. Knothe Tate, *Current insights on the regenerative potential of the periosteum: molecular, cellular, and endogenous engineering approaches.* J Orthop Res, 2012. **30**(12): p. 1869-78.
16. Duchamp de Lageneste, O., et al., *Periosteum contains skeletal stem cells with high bone regenerative potential controlled by Periostin.* Nat Commun, 2018. **9**(1): p. 773.
17. Li, G., et al., *Cell proliferation and apoptosis during fracture healing.* J Bone Miner Res, 2002. **17**(5): p. 791-9.
18. Iwaki, A., et al., *Localization and quantification of proliferating cells during rat fracture repair: detection of proliferating cell nuclear antigen by immunohistochemistry.* J Bone Miner Res, 1997. **12**(1): p. 96-102.
19. Wildemann, B., et al., *Cell proliferation and differentiation during fracture healing are influenced by locally applied IGF-I and TGF-beta1: comparison of two proliferation markers, PCNA and BrdU.* J Biomed Mater Res B Appl Biomater, 2003. **65**(1): p. 150-6.
20. Serowoky, M.A., et al., *Skeletal stem cells: insights into maintaining and regenerating the skeleton.* Development, 2020. **147**(5).
21. Kalajzic, I., et al., *Use of Type I Collagen Green Fluorescent Protein Transgenes to Identify Subpopulations of Cells at Different Stages of the Osteoblast Lineage.* Journal of Bone and Mineral Research, 2002. **17**(1): p. 15-25.
22. Zannit, H.M., M.D. Brodt, and M.J. Silva, *Proliferating osteoblasts are necessary for maximal bone anabolic response to loading in mice.* The FASEB Journal. **n/a**(n/a).
23. Colnot, C., *Skeletal cell fate decisions within periosteum and bone marrow during bone regeneration.* J Bone Miner Res, 2009. **24**(2): p. 274-82.
24. Jilka, R.L., et al., *Intermittent PTH stimulates periosteal bone formation by actions on post-mitotic preosteoblasts.* Bone, 2009. **44**(2): p. 275-86.
25. Gardner, M.J., et al., *Differential fracture healing resulting from fixation stiffness variability: a mouse model.* J Orthop Sci, 2011. **16**(3): p. 298-303.
26. Einhorn, T.A., *The cell and molecular biology of fracture healing.* Clin Orthop Relat Res, 1998. **355**.
27. Bonnarens, F. and T.A. Einhorn, *Production of a standard closed fracture in laboratory animal bone.* J Orthop Res, 1984. **2**(1): p. 97-101.

28. McKenzie, J.A., et al., *Activation of hedgehog signaling by systemic agonist improves fracture healing in aged mice.* Journal of Orthopaedic Research, 2019. **37**(1): p. 51-59.
29. Goldberg, V.M., et al., *Bone grafting: role of histocompatibility in transplantation.* J Orthop Res, 1985. **3**(4): p. 389-404.
30. Oni, O.O.A., *A non-union model of the rabbit tibial diaphysis.* Injury, 1995. **26**(9): p. 619-622.
31. Brownlow, H.C. and A.H. Simpson, *Metabolic activity of a new atrophic nonunion model in rabbits.* J Orthop Res, 2000. **18**(3): p. 438-42.
32. Park, S.H., et al., *Effect of repeated irrigation and debridement on fracture healing in an animal model.* J Orthop Res, 2002. **20**(6): p. 1197-204.
33. Kokubu, T., et al., *Development of an atrophic nonunion model and comparison to a closed healing fracture in rat femur.* J Orthop Res, 2003. **21**(3): p. 503-10.
34. Reed, A.A., et al., *Vascularity in a new model of atrophic nonunion.* J Bone Joint Surg Br, 2003. **85**(4): p. 604-10.
35. Kaspar, K., et al., *A new animal model for bone atrophic nonunion: fixation by external fixator.* J Orthop Res, 2008. **26**(12): p. 1649-55.
36. Tawonsawatruk, T., M. Kelly, and H. Simpson, *Evaluation of native mesenchymal stem cells from bone marrow and local tissue in an atrophic nonunion model.* Tissue Eng Part C Methods, 2014. **20**(6): p. 524-32.
37. Roberto-Rodrigues, M., et al., *Novel rat model of nonunion fracture with vascular deficit.* Injury, 2015. **46**(4): p. 649-54.
38. Wang, L., et al., *Periosteal Mesenchymal Progenitor Dysfunction and Extraskeletally-Derived Fibrosis Contribute to Atrophic Fracture Nonunion.* J Bone Miner Res, 2019. **34**(3): p. 520-532.
39. Bahney, C.S., et al., *Cellular biology of fracture healing.* J Orthop Res, 2019. **37**(1): p. 35-50.
40. Shah, K., et al., *The role of muscle in bone repair: the cells, signals, and tissue responses to injury.* Curr Osteoporos Rep, 2013. **11**(2): p. 130-5.
41. Hausman, M.R., M.B. Schaffler, and R.J. Majeska, *Prevention of fracture healing in rats by an inhibitor of angiogenesis.* Bone, 2001. **29**(6): p. 560-564.
42. Haffner-Luntzer, M., et al., *Mouse Models in Bone Fracture Healing Research.* Current Molecular Biology Reports, 2016. **2**(2): p. 101-111.
43. Hiltunen, A., E. Vuorio, and H.T. Aro, *A standardized experimental fracture in the mouse tibia.* J Orthop Res, 1993. **11**(2): p. 305-12.
44. Holstein, J.H., et al., *Advances in the establishment of defined mouse models for the study of fracture healing and bone regeneration.* J Orthop Trauma, 2009. **23**(5 Suppl): p. S31-8.
45. Kaur, A., S. Mohan, and C.H. Rundle, *A segmental defect adaptation of the mouse closed femur fracture model for the analysis of severely impaired bone healing.* Animal Models and Experimental Medicine. **n/a**(n/a).
46. Buettmann, E.G. and M.J. Silva, *Development of an in vivo bone fatigue damage model using axial compression of the rabbit forelimb.* J Biomech, 2016. **49**(14): p. 3564-3569.
47. Uthgenannt, B.A., et al., *Skeletal self-repair: stress fracture healing by rapid formation and densification of woven bone.* Journal of bone and mineral research : the official journal of the American Society for Bone and Mineral Research, 2007. **22**(10): p. 1548-1556.